

## Boundary Conditions in the Vicinity of a Dynamic Contact Line: Experimental Investigation of Viscous Drops Sliding Down an Inclined Plane

E. Rio, A. Daerr, B. Andreotti, and L. Limat

*Laboratoire de Physique et de Mécanique des Milieux Hétérogènes, UMR CNRS 7636, 10 rue Vauquelin, 75005 Paris, France\**

(Received 2 July 2004; published 21 January 2005)

To probe the microscopic balance of forces close to a moving contact line, the boundary conditions around viscous drops sliding down an inclined plane are investigated. At first, the variation of the contact angle as a function of the scale of analysis is discussed. The dynamic contact angle is measured at a scale of  $6\ \mu\text{m}$  all around sliding drops for different volumes and speeds. We show that it depends only on the capillary number based on the local liquid velocity, measured by particle tracking. This velocity turns out to be normal to the contact line everywhere. It indirectly proves that, in comparison with the divergence involved in the normal direction, the viscous stress is not balanced by intermolecular forces in the direction tangential to the contact line, so that any motion in this last direction gets damped.

DOI: 10.1103/PhysRevLett.94.024503

PACS numbers: 47.10.+g, 68.08.Bc

It has been known from the 19th century that the shape of a sessile drop is controlled by the balance between capillary forces and gravity, together with a boundary condition on the equilibrium contact angle  $\theta_e$  between the liquid and the solid. Minimizing the free energy, one obtains the drop shape and the Young-Laplace equation  $\cos\theta_e = (\gamma_{sg} - \gamma_{ls})/\gamma$  relating  $\theta_e$  to the surface tensions  $\gamma_{sg}$ ,  $\gamma_{ls}$ , and  $\gamma_{lg} = \gamma$  between the solid ( $s$ ), the liquid ( $l$ ), and the gas ( $g$ ). By contrast, there is a lack of understanding of this shape and, in particular, of the boundary conditions at the contact line [1], as soon as the drop moves.

A first difficulty appears already with classical hydrodynamics, which predicts an unbalanced divergence of the viscous stress in the vicinity of the contact line that should prevent any motion [2]. Then, one usually invokes the presence of nanometric molecular effects (slip length, van der Waals forces exerted by substrate molecules, molecular kinetic, diffuse nature of the interface, etc.) to explain the common observation that drops can move [3–8]. Macroscopically, the balance between capillary and viscous forces results in a deviation of the contact angle from its equilibrium value. The situation usually considered theoretically is a two-dimensional liquid film advancing or receding on a substrate. The dynamical angle  $\theta$  is therefore related to the capillary number  $\text{Ca} = \frac{\eta U}{\gamma}$  defined as the speed  $U$  rescaled by the surface tension  $\gamma$  and the viscosity  $\eta$  of the liquid. This relation has been previously determined experimentally in the case of total [9] and partial wetting [10]. It actually depends on the scale at which the measurements are performed [11]. This dependence will be checked profiling a drop with a resolution of  $30\ \mu\text{m}$ .

Our aim, however, is to determine what the correct boundary conditions are in the fully three-dimensional case. What happens if the contact line makes an angle with respect to the overall direction of propagation and thus to the velocity far from it? What determines the

contact angle around a moving droplet, whose contact line continuously changes direction? Does the flow inside the droplet look like a caterpillar, the fluid velocity being aligned in the direction of motion? Here we investigate the boundary conditions (contact angle and velocity) of an inclined moving contact line in the most general case, aiming at deducing microscopic information from these macroscopic measurements.

*Experimental setup.*—Drops of controlled volume are deposited at the top of a glass plate inclined by an angle  $\alpha$ . The liquid used is silicone oil ( $\eta = 50\ \text{cP}$  and  $\gamma = 0.02\ \text{N m}^{-1}$ ), and the glass plate is covered with a fluoropolymer (FC725 sold by 3M) to be in condition of partial wetting. The irregularities of coating have a size around the optic wavelength (a few iridescence fringes visible over  $1\ \text{cm}$ ). The wetting hysteresis is then about  $7^\circ$ , which is quite small and probably due to chemical heterogeneity. The size of the drops and the inclination angle  $\alpha$  determine the capillary number, which is measured directly. The shape of droplets sliding down such a plate has already been investigated with the same setup [12]. They are rounded at small  $\text{Ca}$ , a corner appears at the back for a critical value  $\text{Ca}_c$ , and, above, drops start to pearl. We recovered the same shape transition for larger drops flattened by gravity, i.e., for puddles of about  $1\ \text{cm}^3$ . Typical examples are displayed in Figs. 3(a) and 1(b) (a puddle with a corner at the back and a rounded puddle, respectively).

The existence of a well defined dynamic contact angle is not obvious at all, as the viscous stress becomes comparatively more and more important as one gets closer to the contact line, inducing a divergence of the free surface curvature. In order to determine accurately the variation of the contact angle with the scale of analysis, we measured the slope of the free surface using the refraction of a laser beam [13] (Fig. 1, with a laser beam instead of the sheet). A red laser diode (635 nm, 5 mW) is collimated on a thin hole of diameter  $10\ \mu\text{m}$  by a small focal lens. The image of the

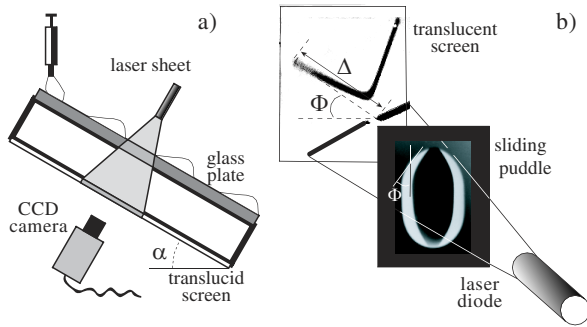


FIG. 1 (color online). (a) A side view sketch of the experimental setup. (b) Principle of the dynamic angle measurement. A laser sheet is refracted at the free surface of the drop and then illuminates a translucent screen, recorded by a charge-coupled device (CCD) camera. Two quantities are derived from each refraction picture, the inclination  $\Phi$  of the contact line with respect to the direction of motion and the maximum deviation  $\Delta$ , which is related to the contact angle. When necessary, the laser sheet is replaced by a single collimated laser beam.

hole is focused at the surface of the glass plate using a projection lens of focal length 50 mm. The laser beam is orientated perpendicular to the plate (Fig. 1). It is refracted at the droplet free surface, crosses the droplet and the glass plate, and finally hits a translucent screen. The position of the spot is recorded with a fast video camera (FastCam  $1024 \times 512$  at 512 Hz), giving an accurate measurement of the refraction angle. As the droplet moves at a constant velocity  $U$ , the refraction angle as a function of time allows one to reconstruct the droplet profile and its slope (see Fig. 2) by solving an integrodifferential problem of geometrical optics—the optical index of the silicone oil (1.4) and the glass plate (1.5) are measured independently.

A typical profile at large capillary number ( $Ca = 5.3 \times 10^{-3}$ ) is shown on Fig. 2. The variation of the slope is not trivial at all: instead of the linear increase of  $\partial_x h$ , with  $x$  expected for a static drop, the curvature is, in the dynamical case, essentially concentrated at the front of the drop.

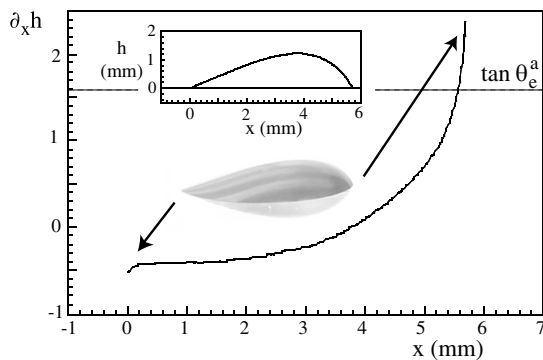


FIG. 2. Local slope  $\partial_x h$  along the central axis of a moving droplet. At the maxima of deviation, the slope is still far from the equilibrium values,  $\tan \theta_e^a \approx 1.6$  and  $\tan \theta_e^r \approx 1.3$  (not shown). Inset: droplet profile determined from the measurements, compared to a direct photograph from the side.

At the back of the droplet, the slope exhibits a sudden decrease when approaching the contact line by less than  $100 \mu\text{m}$ . This is reminiscent of the balance between capillary and viscous forces, which induces a strong curvature of the free surface. It corresponds to the assumption usually made in theoretical studies—and not justified by any serious argument—that the angle at the nanometer scale should be the equilibrium angle  $\theta_e$ . Surprisingly, the angle does not decrease close to the front of the droplet, even at a scale of  $30 \mu\text{m}$ . We therefore observe an asymmetry between the advancing and the receding contact line. It would be interesting to know if this asymmetry is expected theoretically at this scale. The spatial resolution of the contact angle measurement is mostly limited by the displacement of the droplet between two images ( $4 \mu\text{m}$ ) and the diameter of the laser beam on the plate, i.e., at the waist ( $\ell = 30 \mu\text{m}$ ). By comparison, using a side view of the droplet, one can typically resolve only the contact angle to within  $\ell = 200 \mu\text{m}$ . While there is a plateau on the curve at the rear, allowing the definition of a macroscopic contact angle, it is not the case at the front. We have thus chosen to perform the measurements at the lowest scale resolved experimentally.

In a second set of experiments, we measured the contact angle all around the puddle, replacing the laser beam by a laser sheet collimated on the plate [14]. It gives refraction pictures similar to that shown in Fig. 1(b), from which two quantities can be extracted: the maximum length  $\Delta$  of the light deviation, which is related to the contact angle  $\theta$  at the smallest scale resolved, and the angle  $\Phi$  between the contact line and the overall direction of motion. Note that the light is deflected perpendicularly to the contact line. The time evolution of the refraction picture—and thus  $\Phi$  and  $\Delta$ —is recorded, while the laser scans the entire puddle. We finally get the contact angle  $\theta$  as a function of the position around the droplet, parametrized by  $\Phi$ . The scale at which the measurement is performed is no longer determined by the laser collimation but by the minimal intensity detectable by the sensitivity of the camera. This gives a limit value to the curvature of the free surface, which itself gives a resolution of  $\ell = 6 \mu\text{m}$ . This also corresponds roughly to the scale at which geometrical optics break down ( $10\lambda$ ).

*Fluid velocity and dynamical angle at the contact line.*—The relation between the dynamic contact angle and the capillary number is plotted in Fig. 3. The first series of measurements (solid symbols) correspond to the classical situation of a contact line perpendicular to the direction of motion, i.e., to the plane slope. At the drop front ( $\Phi = \pi/2$ ), the contact line is advancing, and at the rear ( $\Phi = -\pi/2$ ), it is receding. The corresponding contact angles are measured using the maximum deviation of a laser spot, for different inclination angles  $\alpha$  and different drop volumes. They collapse on a single curve, when plotted as a function of the capillary number ( $-Ca$

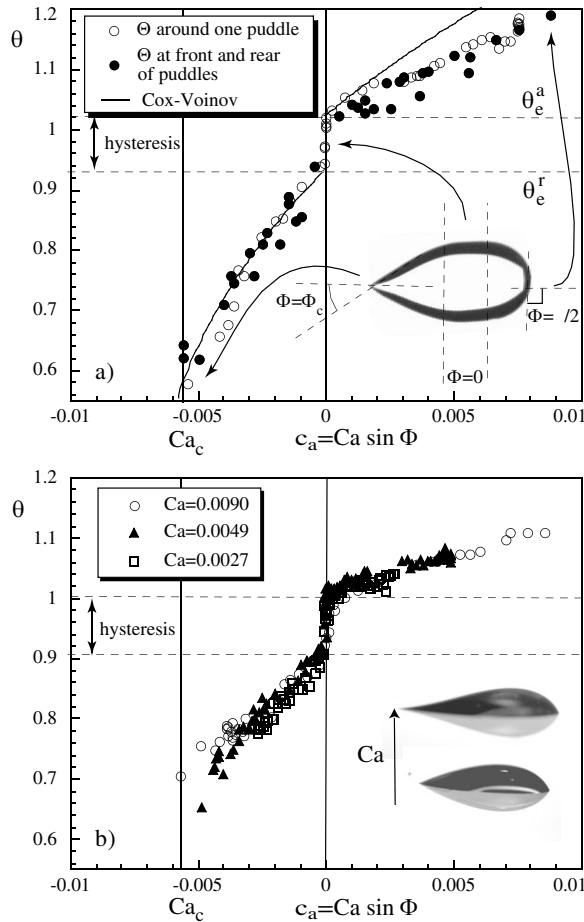


FIG. 3. (a) Contact angle  $\theta$  measured at the front and the back of different puddles as a function of the capillary number  $Ca$  (solid symbols) and around a single puddle as a function of  $ca = Ca \sin \Phi$  (open symbols). Note that there does not exist any receding contact line below the critical capillary number  $Ca_c \approx 5 \times 10^{-3}$ . The solid line corresponds to the best fit by a Cox-Voinov relation for receding contact lines. (b) Superimposition of the contact angle  $\theta(ca)$  around puddles sliding at different capillary numbers ( $Ca = 2.7 \times 10^{-3}$ ,  $Ca = 4.9 \times 10^{-3}$ , and  $Ca = 9.0 \times 10^{-3}$ ). The slight change between the curves in (a) and (b) results from the coating of a new glass plate.

receding lines), indicating that this relationship is local and does not depend much on the bulk (in particular, the curvature at the top of the drop). As previously obtained [9,10,15],  $\theta$  is related to  $Ca$  by a piecewise linear relationship, within the experimental error bars. For negative capillary numbers, we have compared the measurement to the Cox-Voinov prediction [3,4],  $\theta^3 = \theta_c^3 + 9 \ln(\ell/a)Ca$ , as suggested by the presence of a strong decrease of the surface slope close to the contact line (Fig. 2). It gives a nanometric regularization scale  $a$  of the order of 1 Å, as obtained from measurements at the scale of the drop [15]. On the other hand, the same relation does not hold—with the same  $a$ —for advancing contact lines, which is reminiscent of the asymmetry observed on the slope profile (Fig. 2).

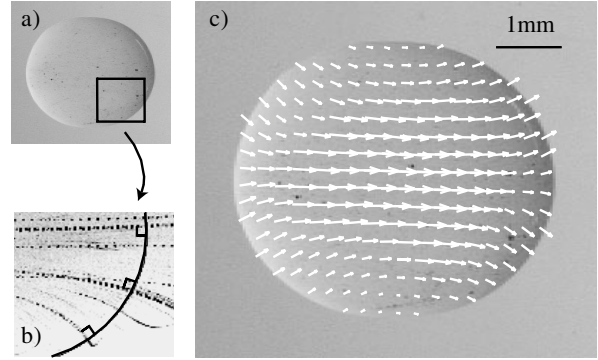


FIG. 4. (a) Visualization of a puddle from the top. Black points are little particles in the puddle. (b) Traces left by the particles while the sliding of the drop superimposed on the puddle's contour. (c) Velocity field in the frame of reference of the plate, measured by particles tracking.

For the sake of comparison, the contact angle  $\theta(\Phi)$  around a single puddle of capillary number  $Ca = 9 \times 10^{-3}$  is also plotted in Fig. 3(a) (open symbols). The best collapse is obtained when  $\theta$  is plotted as a function of a local capillary number  $ca = Ca \sin \Phi$ , previously introduced in the context of corner formation [12,16,17]. Finally, we have varied the speed  $U$  of drops by changing the inclination angle  $\alpha$ . Again the resulting curves  $\theta(ca)$  collapse on the same master curve [Fig. 3(b)]. So, a solid conclusion can be drawn: the mesoscale dynamic contact angle only depends on the capillary number based on the normal velocity of the contact line  $u = U \sin \Phi$ .

This first boundary condition already imposes strong constraints on the shape of the drops. Turning around a drop, the whole curve between  $Ca$  at the front ( $\Phi = \pi/2$ ) and  $-Ca$  at the rear ( $\Phi = -\pi/2$ ) is explored. The existence of an hysteresis implies the existence of a straight portion of contour along the steepest slope of the plane  $\Phi = 0$  where the contact angle covers the hysteresis range [region between the dashed lines in Fig. 3(a)]. Increasing the hysteresis will thus simply lengthen the drop like a “stretched limousine.” Another striking consequence concerns the transition towards the formation of a corner at the back of the drop [12,15,16]. At high capillary numbers, the contact line tilts at the rear, reducing the local capillary number  $ca$  to its critical value  $Ca_c$ . So, according to the boundary condition, the contact angle remains constant and equal to a non-null value  $\theta_c$ . This provides a rigorous basis to the idea of Blake and Ruschak [16] and Podgorski *et al.* [12] that the drop shape change occurs in order to avoid the wetting transition. Now the corner geometry is fully characterized by the opening angle  $\Phi = \arcsin(Ca_c/Ca)$  and the contact angle  $\theta_c$ .

The second boundary condition, which had not been investigated so far, governs the fluid velocity at the interface. To visualize the flow inside the drops, small dye particles are poured on the plate in front of the drop [Fig. 4(a)]. When the drop slides over the particles, the

dye is entrained and marks trajectories along the drop free surface and back to the surface of the plate (null velocity in the frame of reference of the plate). This technique ensures the absence of particles in the bulk. Using particle tracking we measured the whole surface velocity field [Fig. 4(c)]. It turns out that the trajectories are deflected toward the contact line and meet it perpendicularly [Figs. 4(b) and 4(c)]. In the steady state, this means that the local speed of the liquid is normal to the contact line and equal to  $u = U \sin\Phi$ . This justifies the observation that the contact angle  $\theta$  depends only on the local capillary number  $ca = \eta u/\gamma$  and is insensitive to the direction of motion far from the contact line.

*Microscopic interpretation.*—The deviation of the contact angle from its equilibrium value is basically due to the divergence of the viscous stress when approaching the contact line, i.e., when the flow height  $h$  tends to 0. As the Reynolds number tends to 0, we are almost at an equilibrium of viscous forces, capillary forces, and other forces acting on a nanometric scale (slip length, intermolecular forces, evaporation, etc.). Considering an infinitesimal volume of height  $h$  and section  $dx dy$ , it is easy to see that the energy injection rate by gravity,  $\int_V \rho \vec{g} \sin\alpha \vec{u} \approx \rho g U h dx dy$ , becomes negligible with respect to viscous dissipation,  $\eta \int_V (\nabla u)^2 \approx \eta U^2/h dx dy$ , as  $h \rightarrow 0$ . The work produced by surface tension,  $\gamma \int_{\partial V} \kappa u \approx \gamma \int_V \nabla(\kappa u) \approx \gamma \kappa U dx dy$ , can be of the same order of magnitude, provided the curvature  $\kappa$  diverges as  $1/h$ , and nanoscale forces may also counteract the viscous forces. The important point, however, is that in the common situation, most properties vary slowly in the direction tangent to the contact line (say, at the macroscopic scale) while they vary very rapidly in the normal direction. It is the case, for instance, of the surface curvature  $\kappa$  which drastically changes from the micrometric to the millimetric scales along the normal direction (Fig. 2). We can thus neglect any effect associated with the variation of curvature along the contact line, which means that the geometry of the problem can be considered as symmetric with respect to the plane normal to the contact line. Except for the viscous stress, which has the direction of the local velocity  $\vec{u}$ , all the forces important at small scale are thus normal to the contact line. So any fluid motion in the direction tangential to the contact line are efficiently damped by the viscosity, with a time scale  $h^{-2}/\nu \approx 1 \mu s$  for the scale of analysis used here, and the fluid velocity is normal to the contact line. Let us emphasize that this symmetry argument is valid whatever the mechanism balancing the viscosity is. In the hydrodynamic approach, it is the gradient of curvature, whose ratio of normal to tangential component is of the order of the ratio between the macroscopic to the microscopic scale ( $10^3$ – $10^6$ ). If one introduces the intermolecular forces through a disjoining

pressure  $\Pi(h)$ , its gradient  $\vec{\nabla}\Pi = \Pi'(h)\vec{\nabla}h$  is again along the normal direction. The only exception is the case in which there are strong variations along the contact line, namely, the corner at the rear of a drop. Further work is needed to understand the hydrodynamics in this situation and to measure the scale at which this singularity gets regularized [17].

In summary, we have investigated the boundary conditions at an inclined moving contact line. As in the static case, the aim is to solve a macroscopic problem, hiding the microscopic effects into a dynamic contact angle. Once one has fixed the scale  $\ell$  at which the boundary condition is given, we have demonstrated experimentally that there exists a unique relation between the dynamic contact angle and the local capillary number  $ca = \eta u/\gamma$  based on the liquid velocity at the point considered. Moreover, fluid velocity is everywhere normal to the contact line. The challenge is now to use these boundary conditions to determine the shape of sliding droplets and the velocity field inside them, and to understand the formation of a corner at a critical capillary number.

We wish to thank J. Snoeijer and R. V. Roy for helpful discussions.

---

\*Matière et Systèmes Complexes, University Paris 7, FR CNRS 2438, Paris, France.

- [1] E. B. Dussan V, *J. Fluid Mech.* **151**, 1 (1985).
- [2] C. Huh and L. E. Scriven, *J. Colloid Interface Sci.* **37**, 196 (1971).
- [3] O. V. Voinov, *Fluid Dyn.* **11**, 714 (1976).
- [4] R. G. Cox, *J. Fluid Mech.* **168**, 169 (1986).
- [5] P. G. de Gennes, X. Hua, and P. Levinson, *J. Fluid Mech.* **212**, 55 (1990).
- [6] Y. Pomeau, *C. R. Acad. Sci.* **11**, 411 (2000).
- [7] T. D. Blake, J. De Coninck, and U. d'Ortona, *Langmuir* **11**, 4588 (1995).
- [8] Y. Shikhmurzaev, *J. Fluid Mech.* **334**, 211 (1997).
- [9] H. P. Kavehpour, B. Ovryn, and G. H. McKinley, *Phys. Rev. Lett.* **91**, 196104 (2003).
- [10] M. Fermigier and P. Jenffer, *J. Colloid Interface Sci.* **146**, 226 (1991).
- [11] C. G. Ncan and E. B. Dussan V, *J. Fluid Mech.* **118**, 27 (1982).
- [12] T. Podgorski, J.-M. Flesselles, and L. Limat, *Phys. Rev. Lett.* **87**, 036102 (2001).
- [13] C. Redon, F. Brochard-Wyart, and F. Rondelez, *Phys. Rev. Lett.* **66**, 715 (1991).
- [14] E. Rio, A. Daerr, and L. Limat, *J. Colloid Interface Sci.* **269**, 164 (2003).
- [15] N. Le Grand, A. Daerr, and L. Limat (to be published).
- [16] T. D. Blake and K. J. Ruschak, *Nature (London)* **282**, 489 (1979).
- [17] L. Limat and H. Stone, *Europhys. Lett.* **65**, 365 (2002).